Swansea University
Prifysgol Abertawe

Cronfa
Setting Research Free

Cronfa - Swansea University Open Access Repository

_____

This is an author produced version of a paper published in :
Geophysical Research Letters

Cronfa URL for this paper:
http://cronfa.swan.ac.uk/Record/cronfa29287

_____

_____

On the role of buoyant flexure in glacier calving

Till J. W. Wagner[1], Timothy D. James[2], Tavi Murray[2], and Dominic Vella[3]

[1]Scripps Institution of Oceanography, University of California San Diego, San Diego, California, USA, [2]Department of Geography, Swansea University, Swansea, UK, [3]Mathematical Institute, University of Oxford, Oxford, UK

Abstract Interactions between glaciers and the ocean are key for understanding the dynamics of the cryosphere in the climate system. Here we investigate the role of hydrostatic forces in glacier calving. We develop a mathematical model to account for the elastic deformation of glaciers in response to three effects: (i) marine and lake-terminating glaciers tend to enter water with a nonzero slope, resulting in upward flexure around the grounding line; (ii) horizontal pressure imbalances at the terminus are known to cause hydrostatic in-plane stresses and downward acting torque; (iii) submerged ice protrusions at the glacier front may induce additional buoyancy forces that can cause calving. Our model provides theoretical estimates of the importance of each effect and suggests geometric and material conditions under which a given glacier will calve from hydrostatic flexure. We find good agreement with observations. This work sheds light on the intricate processes involved in glacier calving and can be hoped to improve our ability to model and predict future changes in the ice-climate system.

1. Introduction

The accelerated disintegration of Antarctic ice shelves and the retreat of glaciers in all regions of the cryosphere are among the most consequential manifestations of a changing global climate [*Rignot et al.*, 2011, 2013; *Paolo et al.*, 2015]. Rising sea levels, increased ocean temperatures, changing surface albedo, and other positive feedback effects are expected to further increase the rates of melting and decay in the cryosphere [e.g., *Joughin et al.*, 2014; *Mouginot et al.*, 2015]. Interactions between glacier termini or ice shelf fronts and the ocean are therefore regarded as key processes in the dynamics of the cryospheric climate system: the presence or absence of a buttressing ice shelf can determine the stability of vast ice sheets [*Dupont and Alley*, 2005; *Gudmundsson*, 2013], and the oceanic conditions at glacier termini are believed to be among the leading factors in setting glacier flow velocities and calving rates [*Holt et al.*, 2013; *Wouters et al.*, 2015]. Here we examine the role that elastic flexure plays in the calving of floating glacier termini. While the majority of recent modeling studies focus on the appearance and propagation of crevasses as the glacier termini (or ice shelves) advance [e.g., *Nick et al.*, 2010; *Cook et al.*, 2012; *Bassis and Jacobs*, 2013], we revisit the role of purely elastic bending stresses due to hydrostatic imbalances. Building on previous theoretical work by *Reeh* [1968] and *Vaughan* [1995], we consider an idealized representation of the glacier-bedrock-ocean system, in order to maintain a level of simplicity that will yield new insight into the governing physical processes.

The motivation for this work is twofold. First, recent observational results suggest an important role of buoyant flexure in glacier calving under certain conditions [*Benn et al.*, 2007; *Boyce et al.*, 2007; *James et al.*, 2014; *Murray et al.*, 2015a]. In particular, a glacier on a sloped bed will experience an isostacy-driven upward deflection as it enters the water [e.g., *Sayag and Worster*, 2013].

Second, recent work on the breakup of icebergs due to hydrostatic stresses from a submerged ice foot (the "footloose" mechanism) [*Scambos et al.*, 2008; *Wagner et al.*, 2014] prompts the question of whether a similar mechanism might operate at floating glacier fronts. Glaciers terminating in temperate waters are frequently found to feature such underwater feet. The warmer water near the surface leads to higher melting rates in that region, resulting in submerged ice projecting beyond the subaerial face [*Wright and Haynes*, 1892; *Savage*, 2001; *Stern et al.*, 2015]. This effect is expedited by thermal erosion at the water line, which creates a notch in the glacier front [*Röhl*, 2006], leading to an unsupported overburden that eventually collapses [*Benn et al.*, 2007, their Figure 9], leaving behind a submerged foot. Ice blocks have been found to surface 500 m from the terminus of LeConte Glacier in Alaska [*Motyka*, 1997], and submarine ice feet were recently observed to extend to similar distances at lake-terminating glaciers in New Zealand [*Robertson et al.*, 2012].

Greenland's glaciers are often fast flowing and terminate in deep fjords characterized by cold surface water with warmer water at depth [cf. *Straneo et al.*, 2011]. A submerged ice foot as described above then seems unlikely to form. However, observational evidence shows that glacier fronts are irregularly shaped, featuring undercutting near the base but also protrusions out from the calving face [*Rignot et al.*, 2015; *Fried et al.*, 2015] (see also section 3). Since any submerged ice projecting beyond the calving face of the glacier causes an imbalance of buoyancy and weight away from isostasy, irrespective of its shape, we use the general term "protrusion" (rather than "foot") to refer to such ice.

2. Theoretical Model of Buoyant Flexure

We consider a purely elastic model, which presents a good approximation when the glacier advance-calving cycle occurs on time scales that are much shorter than those of viscous creep. *Sayag and Worster* [2013] estimate the viscous bending time scale of ice sheets to be broadly $0.15 < \tau_b < 21$ years. This range suggests that the elastic behavior should dominate viscosity for processes that occur on a time scale faster than $1-2$ months. Calving at Helheim Glacier, for example, as documented by *James et al.* [2014], occurs over at most 4 weeks, and the calving event itself is rapid, which suggests that elastic effects have an important, if not dominant, effect.

To facilitate theoretical progress, we make a number of simplifying assumptions: the glacier is represented as a one-dimensional elastic beam of uniform thickness h and constant material properties (elastic modulus, E, Poisson ratio, ν, and density, ρ_i). Corrections to this model due to the finite thickness of the beam can be found in powers of $\sim (h/l)^2$, where l is the length of the beam [*Timoshenko and Goodier*, 1970]. Here, l is the length of the floating glacier tongue. Ratios of $h/l \approx 3$ are appropriate to the observational examples discussed below, suggesting that the assumption of a thin beam may introduce errors <10%. However, confirming this remains a topic for further work. We ignore any nonuniformity of the system in the direction parallel to the grounding line, as well as vertical or horizontal nonuniformities in the ice (such as cracks, crevasses, or firn). The stress thresholds discussed below should therefore be interpreted as upper bounds on the calving stresses for a given material. We further consider only static mean stresses and will ignore tidal or wave effects, which have been studied in some detail in the past [e.g., *Vaughan*, 1995; *Schmeltz et al.*, 2002; *Sergienko*, 2010; *Sayag and Worster*, 2013].

Two purely elastic models of floating glacier tongues have previously been considered: a "fixed-stiff" model [*Vaughan*, 1995] and the slightly more comprehensive "free-soft" model [*Sayag and Worster*, 2011]. Here the terms "fixed" and "free" refer to whether the grounding line position is seen as given (fixed) or computed as part of the solution (free). "Stiff" and "soft," on the other hand, refer to bedrock of infinite or finite stiffness, respectively. We will briefly revisit these two approaches and then introduce a new model, built on the previous ones, which allows us to consider the combined role that buoyancy-induced stresses play in glacier calving.

2.1. Fixed-Stiff and Free-Soft Elastic Models

The standard fixed-stiff model considers an elastic beam that is freely floating on water at one end and pinned to bedrock at the grounding line. Nevertheless, the shape of the elastic beam, $w(x)$, is not known and must be solved from the floating beam equation [*Holdsworth*, 1969; *Vaughan*, 1995]

$$Bw'''' = -\rho_i g h + \rho_w g(h/2 - w) + Q, \tag{1}$$

where B is the bending stiffness of the "ice beam," defined as $B = Eh^3/12(1-\nu^2)$, ρ_w is the density of water, and g is the gravitational acceleration. $Q(x)$ is an additional force term that usually represents tidal forcing and is therefore often considered to also vary with time. For a free-floating beam $Q=0$ and the boundary conditions at the glacier terminus, x_t, are given by $w''(x_t) = w'''(x_t)=0$. In the presence of an underwater protrusion or undercut, Q will be nonzero and the boundary conditions need to be adjusted accordingly (see below).

The fixed-stiff model was conceived to study the tidal response of long ice shelves [*Vaughan*, 1995]. In that case, the beam can be presumed to rest on flat bedrock up to the fixed grounding point, x_g, giving boundary conditions $w'(x_g) = 0$ and $w(x_g) = w_\infty$. Here w_∞ is the distance between the centerline in isostatic equilibrium and sea level, defined as $w_\infty \equiv h/2 - d$, with the draft $d \equiv (\rho_i/\rho_w)h$.

To study the role that hydrostatic flexure plays in calving, it is necessary to account for the slope of the bedrock near the grounding point (Figure 1). Assuming this slope, S, is approximately constant at some angle θ to the
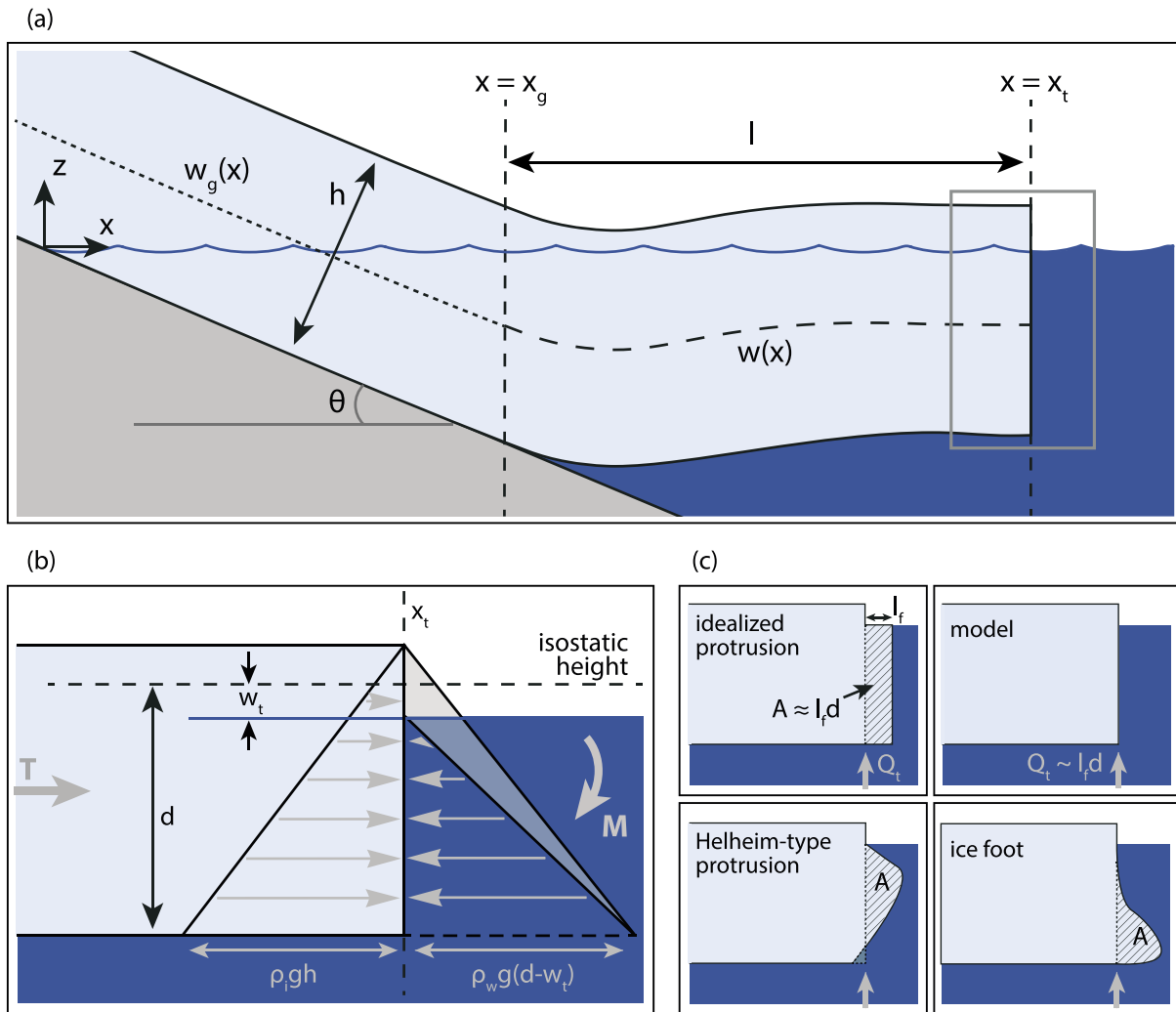
Figure 1. Model setup. (a) Schematic of glacier of thickness h, detaching from a bed of slope θ at $x = x_g$, with terminus at $x = x_t$. The centerline profile of the floating glacier segment (of length l) is $w(x)$, that of the grounded part is $w_g(x)$. The bed is at sea level at $x = 0$. Details shown in Figures 1b and 1c are outlined by the gray box at the glacier front. (b) Detail of the forces (gray arrows) acting at x_t, adapted from *Reeh* [1968]. (c) A submerged protrusion exerts a buoyancy force proportional to its cross-sectional area A at x_t. The four panels illustrate (clockwise from top left): an idealized rectangular protrusion with $A = l_f d$; the model configuration which simulates the added buoyancy as a shear force $Q_t \sim l_f d$; an ice foot, jutting out near the base of the terminus; a protrusion (with undercutting) of similar shape to that observed at Helheim Glacier (see section 3).

horizontal, $S = \tan\theta$, the centerline of the grounded part of the glacier is given by $w_g(x) = h/2 - Sx$; the boundary conditions at the grounding point then become $w(x_g) = h/2 - Sx_g$ and $w'(x_g) = -S$. In this case, the grounding point itself can be found by imposing an additional "ungrounding condition" from the continuity of the bending moment: $w''(x_g) = 0$. This assumes no adhesion between ice and bedrock [*Landau and Lifshitz*, 1986; *Wagner*, 2013].

At the glacier front, the horizontal pressure from the ice is balanced by that of the water only at the bottom of the ice. The unbalanced pressure due to the freeboard (part above the waterline) leads to a net in-plane stress and nonzero torque at x_t (Figure 1b) [*Reeh*, 1968; *Sergienko*, 2010]. In the present framework, this leads to an additional term, $-Tw''(x)$, on the right-hand side of (1), in which T is the constant in-plane tension, computed by integrating the net horizontal pressure at x_t over the beam thickness. Neglecting terms of order $\mathcal{O}(w_t^2)$, this gives $T = \frac{1}{2}\rho_w g \left(hd - d^2 + 2dw_t \right)$, with $w_t \equiv w(x_t) - w_\infty$ [*Reeh*, 1968]. Similarly, the moment at x_t is given by $M = \frac{1}{12}\rho_w g d \left[h^2 - 3dh + 2d^2 + 6w_t (h - d) \right]$. Note that both T and M depend on the deflection of the end, w_t, and are therefore not known a priori. Elastic "thin beam" glacier models commonly neglect this imbalance at
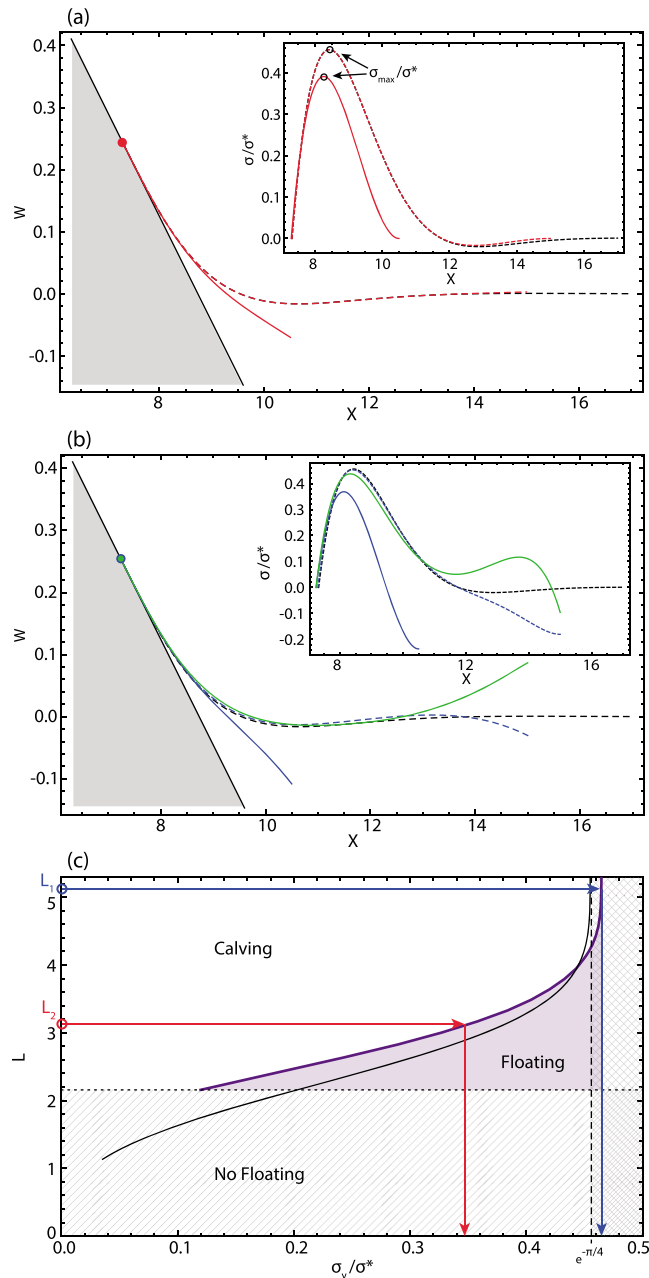
Figure 2. Solutions for a glacier entering water on a sloped bed ($S = 0.17$, $\theta \simeq 9.6°$). (a) Glacier profiles $W(X)$ in the limit $\tau = 0$, for $L = 3.3$ (solid red) and $L = 7.7$ (dashed red). The grounding point is marked by the red dot. The dashed black curve indicates the analytic solution (4). Inset: scaled stresses $\sigma(X)/\sigma^*$, corresponding to the profiles in the main figure. (b) Blue curves are analogous to red curves in 2a but for the full model (2), with $H = 1.65$ (corresponding to the parameters in B07). The green curve illustrates the effect of a submerged protrusion pushing up at the terminus ($L_f = 0.07/D$). (c) Regime diagram of calving: the black curve shows the critical length of a floating tongue, $L_c(\sigma_y/\sigma^*)$, in the limit of thin glaciers and small slopes, where $\tau = 0$. The purple curve gives L_c for the full model (2), with $S = 0.17$ and $H = 1.65$. The half-hatched area gives the parameter space in which the downward deflection of the glacier front outweighs the upward buoyancy, resulting in a grounded terminus. For $\sigma/\sigma^* > e^{-\pi/4}$, the glacier yield strength is too high for calving to occur, regardless of L (cross hatched). The purple, continuously shaded area shows the regime in which a stable floating tongue is possible. Red and blue arrows illustrate the critical yield strengths for calving lengths from Figure 4, L_1 and L_2, respectively.

the glacier front [*Vaughan*, 1995; *Sayag and Worster*, 2011]. Here, however, we find that the resulting stresses are comparable to those from the other buoyancy forces (see below), and so we retain this effect in the present model.

Sayag and Worster [2011] consider a free-soft model, accounting for nonzero slope as well as a finite stiffness in the bed. For the present purposes we take the deformation of the bed to be negligible, assuming that the elastic bending of the ice is energetically cheap, relative to that of the bedrock. We therefore consider a "free-stiff" glacier model that allows for the glacier to enter the water at a nonzero angle, considers the in-plane stress due to the unbalanced freeboard, and treats the grounding point as a free boundary.

2.2. Governing Equations

The problem can be conveniently rescaled using the system's buoyancy length $\ell_w = (B/\rho_w g)^{1/4}$ [*Vaughan*, 1995; *Wagner and Vella*, 2011]. We define $X = x/\ell_w$, $L = l/\ell_w$, $H = h/\ell_w$ and the dimensionless draft of the glacier $D = d/\ell_w = (\rho_i/\rho_w)H$. To simplify notation, we further take $W = (w - w_\infty)/\ell_w$, with $w_\infty \equiv h/2 - d$, as above, and with the exception $W_t = w_t/\ell_w$. Equation (1) can then be written in dimensionless form as

$$W(X) = \begin{cases} D - SX, & X < X_g \quad \text{(grounded)}, \\ -\tau W'' - W'''', & X > X_g \quad \text{(floating)}, \end{cases} \tag{2}$$

where $\tau = \ell_w^2 T/B$ is the dimensionless (hydrostatic) compressive stress in the beam. Assuming X_t is known, six boundary conditions are required to solve (2), with unknown parameters X_g and τ. These boundary conditions are given by

$$W(X_g) = D - SX_g, \quad W'(X_g) = -S, \quad W''(X_g) = 0,$$
$$W(X_t) = -(\tau + b)/D, \quad W''(X_t) = a + bW(X_t), \quad W'''(X_t) = 0, \tag{3}$$

where $a = D\left(H^2 - 3DH + 2D^2\right)/12$ and $b = D(H - D)/2$. The expressions for a and b are readily derived from those above for the tension and moment, T and M, applied by the hydrostatic pressure on the end. For unknown X_t, a further condition is required to ensure that the length of the glacier is fixed, namely, $L_b = \int_{-\infty}^{X_t}\left(1 + \frac{1}{2}W'^2\right)dX$, where the length of the beam, L_b, is given.

Equation (2), subject to boundary conditions (3), can be solved numerically using software packages such as `Mathematica`. To study the bending effect from the sloped bed alone, the horizontal pressure imbalance at X_t is assumed small ($\tau \approx 0$), in which case (2) reduces to the dimensionless form of (1). This solution is approached in the limits of sufficiently large bed slope, S, or sufficiently small thickness, H. Example deflection and stress profiles for the reduced model (1) are shown in Figure 2a. The analogous solutions for the full model (2) are shown in Figure 2b. The figure also illustrates the beam deflection in the limit $X_t \to \infty$ (see section 2.4), and the role a submerged protrusion can play (section 2.5).

2.3. Calving Criterion for Given Slope and Thickness

From elastic beam theory, the largest bending stress σ at any given point X occurs at the beam surfaces $z = \pm h/2$. We have $\sigma(X) = (Y/\ell_w)|W''(X)|$, where $Y = Eh/2(1-v^2)$ is the stretching stiffness of the beam [*Mansfield*, 2005]. For given beam thickness, a natural stress scale exists: $\sigma^* = YS/\ell_w$, allowing us to plot the dimensionless stress profile $\sigma(X)/\sigma^*$ (Figure 2, insets). σ is maximized at some $X = X_{max}$; we define $\sigma(X_{max}) \equiv \sigma_{max}$. We find that σ_{max} initially increases with increasing X_t, until it settles on a constant value in the limit $X_t \gg 1$. In this limit, σ_{max} can be computed analytically (section 2.4); however, for the general solution of the system (2) and (3), σ_{max} has to be found numerically. Assuming that the beam can be characterized by a uniform and constant yield stress, σ_y, fracture will occur if $\sigma_{max} > \sigma_y$: the beam will break when the maximum stress, σ_{max}, surpasses the material strength σ_y. Since σ_{max} increases with X_t, σ_{max} first reaches σ_y at a critical calving length, L_c, of the glacier tongue. Figure 2c shows the computed dependence of $L_c(\sigma_y/\sigma^*)$ for the full model (purple) with $S = 0.17$ and $H = 1.65$, (corresponding to observed values at Mendelhall Glacier, *Boyce et al.* [2007]) and for the limit $\tau = 0$ (black). The latter solution is independent of both S and H.

2.4. Limit of Long Tongues, $x_t \gg \ell_w$ ($X_t \gg 1$)

To gain further insight into the flexural effect of a long floating tongue (with $X_t \gg 1$) entering water at an angle, we consider the limit $\tau = 0$ and approximate the last two conditions in (3) by $W''(\infty) = W'''(\infty) = 0$. The solution to (1) then takes the form

$$W = \sqrt{2}S\exp\left(\frac{X_g - X}{\sqrt{2}}\right)\cos\left(\frac{X - X_g}{\sqrt{2}}\right), \tag{4}$$
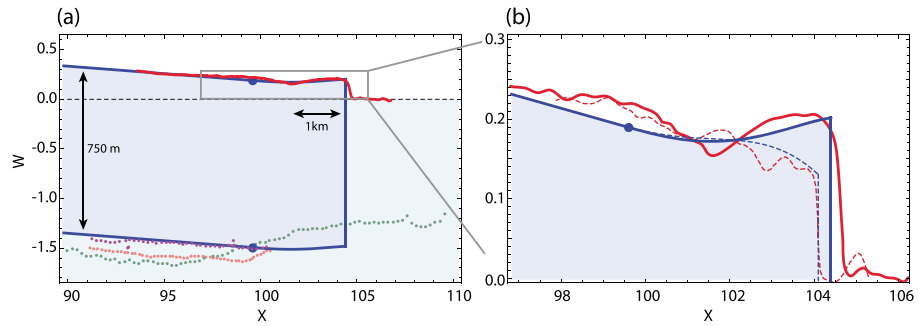
Figure 3. Theoretical and observed glacier profiles. (a) Red curve presents scaled altimetry data, showing the surface of Helheim Glacier on 11 July 2010 (cf. J14, their Figure 1a). Green, purple, and pink dots give CReSIS bed data from 2001, 2011, and 2013, respectively (J14, Figure 4). The modelled outline of the glacier (blue) is computed from (2), including nonzero protrusion. The theoretical grounding point is indicated by blue dots. (b) Detail of terminus region in 3a with additional data (red dashed) from 7 August 2011 (J14, Figure 1c) and the theoretical prediction without a protrusion (dashed blue).

with $X_g = D/S - \sqrt{2}$. This means that the grounding point is located "upstream" of the point of isostacy, $X_i \equiv D/S$. We further find $W(X_g) = \sqrt{2}S$, implying that the glacier is lifted up with respect to its isostatic height by an amount proportional to the slope of the bed.

From (4) it is readily shown that the maximum stress occurs at $X(\sigma_{max}) = X_g + \pi/2\sqrt{2}$. This is consistent with the result in *Wagner et al.* [2014], where it was shown that the maximum stress in a floating beam subject to a point force is found at a dimensionless distance $\pi/2\sqrt{2}$ from the locus of the force. The corresponding maximum stress is $\sigma_{max} = YSe^{-\pi/4}/\ell_w$, or $\sigma_{max}/\sigma^* = e^{-\pi/4}$. As a result, we expect that if $\sigma_y/\sigma^* > e^{-\pi/4}$, the beam will not break from flexure, regardless of its length (Figure 2c). Dimensionally, we obtain the fracture criterion

$$\sigma_{max} = \frac{E}{2(1-\nu^2)}\frac{h}{\ell_w}Se^{-\pi/4} > \sigma_y, \tag{5}$$

which is analogous to fracture criteria previously derived, for example, for rafted sea ice floes [cf. *Parmerter*, 1975; *Vella and Wettlaufer*, 2008].

Equation (5) can be rewritten to give a critical bedrock inclination, S_c, at which calving will occur for given material parameters: We find that the glacier will only calve if $S > S_c \approx 4.39(1-\nu^2)(\sigma_y/E)(\ell_w/h)$. Standard material parameter values for glacial ice are $\sigma_y \sim 10^5 - 10^6$ Pa and $E \sim 10^8 - 10^{10}$ Pa [*Schulson*, 1999], giving $\sigma_y/E \sim 10^{-5} - 10^{-2}$. The fact that these estimates span 3 orders of magnitude illustrates the large variations in glacial ice strength. This is due to a number of fa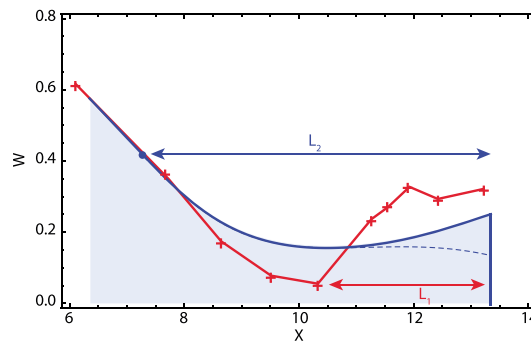ctors, most prominently the degree of crevassing which is highly variable not only between glaciers but also within a single glacier [cf. *Murray et al.*, 2015a]. As an upper bound for very strong and flexible ice ($\sigma_y = 10^6$, $E = 10^8$), we find that the glacier can calve due to flexural stresses if $S \gtrsim 0.04\ell_w/h$. For $E = 10^8$ Pa we find that a glacier like the lake-terminating Mendelhall Glacier, with $h = 75$ m [*Boyce et al.*, 2007], has $\ell_w = 139$ m and the much thicker Helheim Glacier, with $h = 740$ m [*James et al.*, 2014], has $\ell_w = 778$ m. This means that flexural stresses alone are sufficient to cause calving if S(Mendelhall) $\gtrsim 0.07$ and S(Helheim) $\gtrsim 0.04$. From the bathymetry of Mendelhall Lake [*Boyce et al.*, 2007] one finds $S \simeq 0.08$, which suggests that the resulting flexural stresses are sufficient for calving. For Helheim Glacier, we estimate $S \simeq 0.01 - 0.03$ [*James et al.*, 2014], which is

Figure 4. Scaled observational surface profile from Mendelhall Glacier (red, digitized from B07, their Figure 6a) and theoretical curves with protrusion (solid blue) and without (dashed blue). Also indicated are the theoretical tongue length, L_2, and a speculated shorter tongue with grounding point near $X = 10$, (L_1), as indicated in Figure 2c.

slightly lower than the calving limit $S_c = 0.04$. However, using the value $\sigma_y = 10^5$ Pa, taken from *Bassis and Jacobs* [2013], gives S_c(Helheim) = 0.007, in which case the measured slopes would be more than sufficient to cause calving.

In the limit of small S, the bending stresses in the glacier will become less important and other decay mechanisms, such as thermal erosion and strain thinning will dominate the conditions near the glacier front [*Dupont and Alley*, 2005; *Benn et al.*, 2007]. This is also the case for thin glaciers, since $S_c \propto h^{-1/4}$: an increasingly steep bed is required to cause calving from hydrostatic forces as h becomes small, so in practice other mechanisms must take over.

2.5. Effects of an Underwater Protrusion

Above we argued that the glacier's elastic deformation from sloped bedrock alone may induce calving. In what follows, we show how the elastic stresses can be amplified by the presence of submerged ice projecting beyond the subaerial glacier front. The effect of such a protrusion, exerting an upward shear force Q_t at the glacier terminus can be accounted for by changing the final condition in (3) to $W'''(X_t) = Q_t$, where Q_t is proportional to the protrusion's cross-sectional area [*Wagner et al.*, 2014]. We assume here that the protrusion can be approximated by a rectangular shape (Figure 1c), so that $Q_t = L_f D$, where L_f is the dimensionless distance of projection. This simplifies the interpretation of Q_t, but for more realistic shapes it is the value of Q_t that matters. For finite X_t, the emergence of a protrusion can either increase the stress maximum near the grounding point or, for sufficiently long X_t, induce a second stress maximum close to the glacier terminus (Figure 2b, inset). In the limit $X_t \gg 1$ and setting $\tau = 0$, the deformation near the terminus reduces to that of a free-floating iceberg, discussed in *Wagner et al.* [2014], and the deformation near the grounding line reduces to (4).

Note that the model can also capture the flexural response of the glacier due to undercutting, in which case a downward force, $-Q_t$, proportional to the cross-sectional area of the undercut, acts at the terminus.

3. Comparison to Observed Glacier Profiles

Figures 3 and 4 show comparisons between previously reported observational data from *James et al.* [2014] (henceforth J14) and *Boyce et al.* [2007] (henceforth B07) and the theoretical solutions derived in section 2. The glacier and bed profile data has been rescaled by ℓ_w to be presented in dimensionless variables W and X, with $\ell_w = 445$ m and 42 m, for J14 and B07, respectively. These values of ℓ_w are computed using elastic moduli that were chosen to give the best visual match between observational and theoretical profiles ($E = 10^7$ Pa for J14 and $E = 10^6$ Pa for B07).

Figure 3a shows the J14 data curve from 11 July 2010 (solid red), featuring a pronounced upward turning profile (or "rampart-moat" profile [*Scambos et al.*, 2005]). The terminus detail shown in Figure 3b additionally gives the J14 profile from 7 August 2011 (dashed red), which exhibits a monotonic downward slope toward the terminus. This downward turning profile agrees well with a theoretical profile that features no underwater protrusion (blue dashed). However, to understand the upward turning profile observed on 11 July 2010 requires a protrusion to be incorporated in the model (solid blue). The fitted buoyancy force exerted by the protrusion is $L_f D = 0.043$, which corresponds to an average projecting length $l_f = 13$ m.

Time-lapse imagery of a calving event at Helheim Glacier indicates a protrusion in the upper submerged part of the overturning iceberg that calves off the glacier. Three annotated frames are provided in the supporting information (SI), showing a protrusion akin to the schematic in Figure 1c; a video of the event is provided in J14 (their SI). As expected, the deepest parts of this iceberg also show evidence of undercutting, complicating the relatively idealized analysis presented here.

While the origin of submerged protrusions for glaciers flowing into warmer waters is readily explained (see section 1), the cause of a protrusion at Helheim Glacier is less certain. In particular, the oceanographic conditions at Helheim do not support the type of thermal erosion that is known to lead to the footloose mechanism. The presence of a perennial ice mélange would preclude the creation of a notch in the glacier front, which is known to expedite the erosion of the freeboard and lead to a protrusion. Furthermore, water column observations of Helheim Fjord have shown a persistent warm layer of Atlantic water at depth [*Straneo et al.*, 2011], which supports the idea of enhanced undercutting. Nevertheless, the growth of a moderately sized submarine protrusion is plausible for several reasons: air temperatures

in July around Helheim are significantly above melting: the weather station in Tasiilaq reported an average air temperature of 7.4°C for July 2011 (Danish Meteorological Institute, 2011). This, together with observed rainfall of 100 mm in July–August 2011, may have led to enhanced freeboard erosion at the terminus. In general, frequent gravity-driven small-magnitude freeboard calving is often observed in glaciers, compared to less frequent but larger-scale submarine calving [*Warren et al.*, 1995; *Glowacki et al.*, 2015].

Figure 4 presents a comparison between observational surface profile data of Mendenhall Glacier from B07 (red) and two theoretical fits: one without a protrusion (dashed blue) and one with a protrusion (solid blue), the latter of which matches the observational profile more closely.

The agreement between our theory and the observations from J14 and B07 is subject to a number of conditions: (i) The value of the Young's Modulus, E, and the buoyant cross-section of the hypothesized protrusion, $L_f D$, have been fitted to give the best visual match with observations; (ii) the theoretical, constant, bed slopes present rough and idealized estimates ($S = 0.015$ for J14 and $S = 0.17$ for B07, based on the data shown in these studies); (iii) there exist substantial nonuniformities along the glacier fronts, and for both Mendenhall and Helheim Glacier, the front is only partially ungrounded; (iv) we do not account for the likely important role that basal crevasses play in determining the strength of the glacier and the point of fracture [cf. *Murray et al.*, 2015a, 2015b]; and (v) the large uncertainties in the bed data, discussed in J14 and evidenced by the disparate measurements shown in Figure 3a, present a further complication: instead of a steadily sloped bed, the glacier might encounter a pinning point (e.g., in the form of retrograde bed slope) or an abrupt deepening in bathymetry.

A more comprehensive assessment of the theory developed above is made difficult by the scarcity of observational data. Frontal profiles of glaciers calving into warmer waters, together with basal topography, could provide particularly valuable insight and a quantitative test of our theory without the fitting that has been necessary here. In the case of Mendenhall Glacier, two further processes might be expected to play a significant role in setting the hydrostatic balance: the observed rapid thinning of the lower glacier, which can reach rates in excess of 2 m/yr [*Motyka et al.*, 2002] and fluctuations in lake level (discussed in B07). Note that in our (quasi-static) theoretical framework, a rise in lake level is equivalent to the glacier advancing into correspondingly deeper waters and does not change our results quantitatively.

Figure 2c illustrates how two possible critical calving lengths for the B07 profile (L_1 and L_2 in Figure 4) correspond to the nominal yield stress, σ_y/σ^*. In general, this relation can be used to give theoretical estimates of either the yield stress (for known l at calving) or the likely location of calving (for known σ_y).

4. Conclusion

We have shown how the flexure imposed by a glacier entering water at an angle leads to an upward deflection of the glacier front and tensile stresses at its base. These effects can be amplified by a submerged protrusion at the glacier front. Warm air or surface water conditions may cause the freeboard at the glacier front to erode more quickly than the submerged ice, resulting in a steadily growing protrusion that leads to additional flexure and basal tensile stress. When a critical stress level is reached, the glacier will calve not far from the grounding line, leaving behind a vertical face and a monotonic surface profile. Over time, the flow of the glacier will produce another floating section, and the differential melt at the face will lead to the regrowth of the underwater protrusion — the calving cycle repeats itself.

We emphasize that the elastic model presented here is perhaps the simplest that captures the essential features. Future work should revisit this model, going beyond beam theory. We hope that the physical mechanisms discussed here, together with the corresponding theoretical model will complement and inform computationally advanced numerical models, as well as aid the interpretation of observational findings. Bringing these methods closer together is one of the main goals of this study.

References

Bassis, J. N., and S. Jacobs (2013), Diverse calving patterns linked to glacier geometry, *Nat. Geosci.*, 6(10), 833–836.
Benn, D. I., C. R. Warren, and R. H. Mottram (2007), Calving processes and the dynamics of calving glaciers, *Earth Sci. Rev.*, 82(3–4), 143–179.
Boyce, E. S., R. J. Motyka, and M. Truffer (2007), Flotation and retreat of a lake-calving terminus, Mendenhall Glacier, Southeast Alaska, USA, *J. Glaciol.*, 53(181), 211–224.
Cook, S., T. Zwinger, I. C. Rutt, S. O'Neel, and T. Murray (2012), Testing the effect of water in crevasses on a physically based calving model, *Ann. Glaciol.*, 53(60), 90–96.

Dupont, T. K., and R. B. Alley (2005), Assessment of the importance of ice-shelf buttressing to ice-sheet flow, *Geophys. Res. Lett.*, *32*, L04503, doi:10.1029/2004GL022024.

Fried, M. J., G. A. Catania, T. C. Bartholomaus, D. Duncan, M. Davis, L. A. Stearns, J. Nash, E. Shroyer, and D. Sutherland (2015), Distributed subglacial discharge drives significant submarine melt at a Greenland tidewater glacier, *Geophys. Res. Lett.*, *42*, 9328–9336, doi:10.1002/2015GL065806.

Glowacki, O., G. B. Deane, M. Moskalik, P. Blondel, J. Tegowski, and M. Blaszczyk (2015), Underwater acoustic signatures of glacier calving, *Geophys. Res. Lett.*, *42*, 804–812, doi:10.1002/2014GL062859.

Gudmundsson, G. H. (2013), Ice-shelf buttressing and the stability of marine ice sheets, *Cryosphere*, *7*(2), 647–655.

Holdsworth, G. (1969), Flexure of a floating ice tongue, *J. Glaciol.*, *8*, 385–397.

Holt, T. O., N. F. Glasser, D. J. Quincey, and M. R. Siegfried (2013), Speedup and fracturing of George VI Ice Shelf, Antarctic Peninsula, *Cryosphere*, *7*(3), 797–816.

James, T. D., T. Murray, N. Selmes, K. Scharrer, and M. O'Leary (2014), Buoyant flexure and basal crevassing in dynamic mass loss at Helheim Glacier, *Nat. Geosci.*, *7*(8), 593–596.

Joughin, I., B. E. Smith, and B. Medley (2014), Marine ice sheet collapse potentially under way for the Thwaites Glacier Basin, West Antarctica, *Science*, *344*(6185), 735–738.

Landau, L. D., and E. M. Lifshitz (1986), *Theory of Elasticity*, Elsevier, Amsterdam.

Mansfield, E. H. (2005), *The Bending and Stretching of Plates*, Cambridge Univ. Press, New York.

Motyka, R. J. (1997), Deep-water calving at Le Conte glacier, southeast Alaska, in *Calving Glaciers: Report of a Workshop, Byrd Polar Research Centre Report*, vol. 15, edited by C. J. Van der Veen, pp. 115–118, The Ohio State Univ., Columbus.

Motyka, R. J., S. O'Neel, C. L. Connor, and K. A. Echelmeyer (2002), Twentieth century thinning of Mendenhall Glacier, Alaska, and its relationship to climate, lake calving, and glacier run-off, *Global Planet. Change*, *35*(1–2), 93–112.

Mouginot, J., E. Rignot, B. Scheuchl, I. Fenty, A. Khazendar, M. Morlighem, A. Buzzi, and J. Paden (2015), Fast retreat of Zachariæ Isstrøm, northeast Greenland, *Science*, *350*(6266), 1357–1361, doi:10.1126/science.aac7111.

Murray, T., N. Selmes, T. D. James, S. Edwards, I. Martin, T. O'Farrell, R. Aspey, I. Rutt, M. Nettles, and T. Bauge (2015a), Dynamics of glacier calving at the ungrounded margin of Helheim Glacier, southeast Greenland, *J. Geophys. Res. Earth Surf.*, *120*, 964–982, doi:10.1002/2015JF003531.

Murray, T., et al. (2015b), Reverse glacier motion during iceberg calving and the cause of glacial earthquakes, *Science*, *349*(6245), 305–308.

Nick, F. M., C. J. van der Veen, A. Vieli, and D. I. Benn (2010), A physically based calving model applied to marine outlet glaciers and implications for the glacier dynamics, *J. Glaciol.*, *56*(199), 781–794.

Paolo, F. S., H. A. Fricker, and L. Padman (2015), Volume loss from Antarctic ice shelves is accelerating, *Science*, *348*(6232), 327–331.

Parmerter, R. R. (1975), A model of simple rafting in sea ice, *J. Geophys. Res.*, *80*(15), 1948–1952.

Reeh, N. (1968), On the calving of ice from floating glaciers and ice shelves, *J. Glaciol.*, *7*, 215–232.

Rignot, E., I. Velicogna, M. R. van den Broeke, A. Monaghan, and J. Lenaerts (2011), Acceleration of the contribution of the Greenland and Antarctic ice sheets to sea level rise, *Geophys. Res. Lett.*, *38*, L05503, doi:10.1029/2011GL046583.

Rignot, E., S. Jacobs, J. Mouginot, and B. Scheuchl (2013), Ice-shelf melting around Antarctica, *Science*, *341*(6143), 266–270.

Rignot, E., I. Fenty, Y. Xu, C. Cai, and C. Kemp (2015), Undercutting of marine-terminating glaciers in West Greenland, *Geophys. Res. Lett.*, *42*, 5909–5917, doi:10.1002/2015GL064236.

Robertson, C. M., D. I. Benn, M. S. Brook, I. C. Fuller, and K. A. Holt (2012), Subaqueous calving margin morphology at Mueller, Hooker and Tasman glaciers in Aoraki/Mount Cook National Park, New Zealand, *J. Glaciol.*, *58*(212), 1037–1046.

Röhl, K. (2006), Thermo-erosional notch development at fresh-water-calving Tasman Glacier, New Zealand, *J. Glaciol.*, *52*(177), 203–213.

Savage, S. B. (2001), Aspects of iceberg deterioration and drift, in *Geomorphological Fluid Mechanics, Lect. Notes Phys. Ser.*, vol. 582, edited by N. J. Balmforth and A. Provenzale, pp. 279–318, Springer, Berlin.

Sayag, R., and M. G. Worster (2011), Elastic response of a grounded ice sheet coupled to a floating ice shelf, *Phys. Rev. E*, *84*(3), 036111.

Sayag, R., and M. G. Worster (2013), Elastic dynamics and tidal migration of grounding lines modify subglacial lubrication and melting, *Geophys. Res. Lett.*, *40*, 5877–5881, doi:10.1002/2013GL057942.

Scambos, T., O. Sergienko, A. Sargent, D. MacAyeal, and J. Fastook (2005), ICESat profiles of tabular iceberg margins and iceberg breakup at low latitudes, *Geophys. Res. Lett.*, *32*, L23S09, doi:10.1029/2005GL023802.

Scambos, T., R. Ross, R. Bauer, Y. Yermolin, P. Skvarca, D. Long, J. Bohlander, and T. Haran (2008), Calving and ice-shelf break-up processes investigated by proxy: Antarctic tabular iceberg evolution during northward drift, *J. Glaciol.*, *54*(187), 579–591.

Schmeltz, M., E. Rignot, and D. MacAyeal (2002), Tidal flexure along ice-sheet margins: Comparison of InSAR with an elastic-plate model, *Ann. Glaciol.*, *34*, 202–208.

Schulson, E. M. (1999), The structure and mechanical behavior of ice, *JOM*, *51*, 21–27, Springer.

Sergienko, O. V. (2010), Elastic response of floating glacier ice to impact of long-period ocean waves, *J. Geophys. Res.*, *115*, F04028, doi:10.1029/2010JF001721.

Stern, A. A., et al. (2015), Wind-driven upwelling around grounded tabular icebergs, *J. Geophys. Res. Oceans*, *120*, 5820–5835, doi:10.1002/2015JC010805.

Straneo, F., R. G. Curry, D. A. Sutherland, G. S. Hamilton, C. Cenedese, K. Våge, and L. A. Stearns (2011), Impact of fjord dynamics and glacial runoff on the circulation near Helheim Glacier, *Nat. Geosci.*, *4*(5), 322–327.

Timoshenko, S. P., and J. N. Goodier (1970), Theory of Elasticity, 3rd ed., 567 pp., McGraw-Hill, New York.

Vaughan, D. G. (1995), Tidal flexure at ice shelf margins, *J. Geophys. Res.*, *100*(B4), 6213–6224.

Vella, D., and J. S. Wettlaufer (2008), Explaining the patterns formed by ice floe interactions, *J. Geophys. Res.*, *113*, C11011, doi:10.1029/2008JC004781.

Wagner, T. J. W. (2013), Elastocapillarity: Adhesion and large deformations of thin sheets, PhD thesis, Univ. of Cambridge, Cambridge, U. K.

Wagner, T. J. W., and D. Vella (2011), Floating carpets and the delamination of elastic sheets, *Phys. Rev. Lett.*, *107*(4), 044301.

Wagner, T. J. W., P. Wadhams, R. Bates, P. Elosegui, A. Stern, D. Vella, P. Abrahamsen, A. Crawford, and K. W. Nicholls (2014), The "footloose" mechanism: Iceberg decay from hydrostatic stresses, *Geophys. Res. Lett.*, *41*, 5522–5529, doi:10.1002/2014GL060832.

Warren, C. R., N. F. Glasser, S. Harrison, V. Winchester, A. R. Kerr, and A. Rivera (1995), Characteristics of tide-water calving at Glaciar San Rafael, Chile, *J. Glaciol.*, *41*(138), 273–289.

Wouters, B., A. Martin-Español, V. Helm, T. Flament, J. M. van Wessem, S. R. M. Ligtenberg, M. R. van den Broeke, and J. L. Bamber (2015), Dynamic thinning of glaciers on the Southern Antarctic Peninsula, *Science*, *348*(6237), 899–903.

Wright, G. F., and H. W. Haynes (1892), *Man and the Glacial Period*, D. Appleton, New York.

Erratum

In the originally published version of this article, several instances of text were incorrectly typeset. The following have since been corrected and this version may be considered the authoritative version of record.

Section 2.1, paragraph 4, sentence 4 (text insertion '$-w_\infty$'). "This gives $T = \frac{1}{2}\rho_w g\left(hd - d^2 + 2dw_t\right)$, with $w_t \equiv w(x_t)$", was changed to "This gives $T = \frac{1}{2}\rho_w g\left(hd - d^2 + 2dw_t\right)$, with $w_t \equiv w(x_t) - w_\infty$"

Section 2.2, paragraph 1, sentence 2 (text insertion ', and with the exception $W_t = w_t/\ell_w$.') "To simplify notation, we further take $W = (w - w_\infty)/\ell_w$, with $w_\infty \equiv h/2 - d$, as above." was changed to "To simplify notation, we further take $W = (w - w_\infty)/\ell_w$, with $w_\infty \equiv h/2 - d$, as above, and with the exception $W_t = w_t/\ell_w$."